# Greener carbon capture using microwave heating for the development of cellulose-based adsorbents

Simba Biti[a], Alan J. McCue[b], Davide Dionisi[a], Inês Graça[a,c], Claudia Fernández Martín[*a, c]

[a] School of Engineering, Chemical Processes and Materials Engineering Group, University of Aberdeen, Aberdeen AB24 3UE, UK

[b] Department of Chemistry, University of Aberdeen, AB24 3UE

[c] Centre for Energy Transition, University of Aberdeen, United Kingdom

Corresponding author: cfmartin@abdn.ac.uk

**Abstract**

In this work, $CO_2$-activated carbons were produced from microcrystalline cellulose using microwave heating during activation. Activations were thus completed at 400°C to burn-offs of 10, 20 and 30 wt %. The activated carbons' $CO_2$ adsorption capacity was tested over 10 cycles of adsorption (25 °C) and desorption (100 °C). $CO_2$ adsorption capacity was found to increase with increasing activation burn-off, whilst larger average dynamic adsorption capacities were achieved with activated carbons of 20 wt % (1.64 mmol/g) and 30 wt % (1.73 mmol/g) burn-off compared to commercial activated carbon Norit R2030CO2 (1.58 mmol/g). These microwave-prepared activated carbons were also compared with similar activated carbons produced using conventional heating in our previous work. The microwave-prepared activated carbons were found to possess 9.5-25.6 % larger $CO_2$ adsorption capacities at equivalent burn-offs, despite being produced at 200°C lower temperature, 83-94 % shorter activation times and 39-68 % lower heating energy consumption. These results represent the

establishing of a more efficient means of producing microcrystalline cellulose-based activated carbons for a greener, sustainable carbon capture that contributes to the circular economy.

## 1. Introduction

Multiple technological solutions are being explored currently in order to abate $CO_2$ emissions in the atmosphere and deliver a sustainable energy transition. This is in line with decisive decisions made at the 2021 UN COP 26 conference to achieve global net zero $CO_2$ emissions by 2050 and to limit the global temperature increase to 1.5°C [1][2]. Some of the $CO_2$ abatement technologies being explored include Direct Air Capture (DAC), Chemical Looping Combustion (CLC) and pre-, oxy- and post-combustion capture [2]. When considering these technologies, DAC, whilst of growing prominence, captures low $CO_2$ concentrations from the air (~440 ppm) resulting in a substantially higher energy penalty whereas CLC still lacks commercial readiness [2]. Of the remaining options, post-combustion capture has been identified as the most immediately implementable technology as it can be retrofitted into current GHG-emitting industrial processes [3]. As a result, much research has been dedicated towards optimising the performance of post-combustion capture through the development of appropriate, feasible capturing materials. This includes activated carbons (ACs), porous solid sorbents with can be used in various applications in addition to carbon capture including wastewater treatment, soil enhancement and use in catalytic converters [4] [5] [6]. Various studies have demonstrated the successful production of ACs from lignocellulosic, waste-based feedstocks which can provide additional benefit to the circular economy. This includes feedstocks originating from food waste such as agricultural residues and wood-residues [7] [8]. Whilst liquid amines solvents are used most commonly for capture on a commercial scale, ACs are regarded as more advantageous due to lower energy regeneration requirements, lower operating capital costs, simpler scalability, a tendency not to produce harmful by-

47 products during operation and their applicability over a wide array of temperatures and
48 pressures [9]. These are advantages that are in addition to solid sorbents also being capable
49 of capturing $CO_2$ to a promising standard compared to commercial liquid amine solvents [2].
50 Compared to other solid sorbents such as metal organic frameworks (MOFs), carbon
51 nanotubes (CNTS), and carbon membranes, ACs provide the advantage of greater material
52 durability, less complex and costly synthesis procedures as well as greater capability in
53 capturing $CO_2$ in flue gas streams containing moisture [10].

54 Whilst ACs are promising materials for capturing $CO_2$, a critical part of evaluating their
55 application for post-combustion carbon capture is the development of greener production
56 processes. Maximising the production viability can be achieved by adjusting key experimental
57 parameters such as the activating agent used, the activation temperature and duration. For
58 instance, in our previous work ACs from microcrystalline cellulose (MCC) were produced using
59 moderate activation temperature (600°C) and activation burn-offs of up to 30 wt % as part of
60 improving the process feasibility [11]. Another key point of consideration for the
61 improvement of the process efficiency is using an alternative, more efficient heating source.
62 The use of microwave (MW) heating as an alternative to conventional heating sources has
63 emerged as a potential pathway to more efficient production of ACs for $CO_2$ capture [12] [13].
64 Unlike conventional heating, which achieves heating by conductive or convective heating,
65 MW heating achieves heating based on the material's response to the microwave radiation
66 that it is subjected to. Solid materials such as lignocellulosic biomass (LCB) feedstocks,
67 biochars or ACs are heated with MW through the interfacial polarisation mechanism, also
68 known as the Maxwell-Wagner-Sillars effect [14]. In this form of MW heating, the material
69 should consist of conductive and non-conductive regions. In line with the principles of dipolar
70 polarisation, the application of electromagnetic radiation to the (polar) material results in the

material's molecules reorientating to remain in phase with the radiation [15]. Amidst this reorientation, an inertia is experienced by the molecules that does not allow sufficient time for reorientation with the electromagnetic field before it changes direction. The subsequent random particle motion that is generated leads to heat generation [15]. Potential benefits with this heating mechanism include a form of material heating that can be quicker, more selective/controllable and thus more efficient. To be emphasised however, is that this is subject to the nature of the material's response to dielectric heating.

This study thus aims at capitalising on the potential of MW heating, through expanding on the work by Biti et al., where promising ACs produced by physical activation were successfully reported using microcrystalline cellulose (MCC) as a feedstock [11]. MCC is a generally attractive renewable feedstock for various commercial applications because it possesses beneficial mechanical properties such as high strength and stiffness [16]. In addition, it is non-toxic and highly biodegradable [16]. More notably, MCC is proven to be obtainable from various lignocellulosic waste sources including cotton waste, paper waste and agricultural waste, hence its use offers the prospect of a valuable contribution to the circular economy [17] [18]. Whilst lignocellulosic feedstocks such as those previously mentioned could be used in their waste form for AC production, the access of these feedstocks individually are more limited by their geographical abundance. Considering the abundance of cellulose, and the abundance of MCC in various waste forms, MCC is a feedstock with greater global accessibility, which is more appropriate to the global challenge of the need for sustainable sorbent production for post-combustion capture [11]. Also, considering the scale of some of the source materials of MCC such oil palm waste, it is worth investigating whether the potential exists for the development of MCC-based sorbents for post-combustion carbon

capture. Then if conversion is proven feasible, there will still be the need to investigate the effect of the impurities in cellulose and MCC on the physicochemical properties of the resultant adsorbents.

However, and to the best of our knowledge, no studies have explored the development of physically activated, MCC-based ACs for $CO_2$ capture using MW heating. Physical activation has been preferred to rule out the use of chemical agents during production that may be harmful to the environment (i.e., strong acids or bases). The development of such ACs represents a more feasible and environmentally friendly approach to AC development for $CO_2$ capture.

## 2. Experimental

### 2.1. AC preparation

Powder MCC supplied by Merck (particle size 51 µm) was used as feedstock for production. ACs were produced in a two-stage procedure involving carbonisation, where the MCC was converted into biochar, and then activation. Biochars were obtained from carbonisation at 500°C as described in our previous work [11].

MW activation was conducted in a Flexiwave Microwave Synthesis System, purchased from Milestone, Italy. The system consists of a 2.45 GHz multimode microwave cavity, 70.5 L in capacity and fitted with a dual magnetron system for the generation of microwaves. The magnetron response is automatically controlled during the experiments to achieve the target temperature by a closed communication loop between the magnetron and the signal that it receives from an IR sensor (measured sample temperature). The sample temperature and the incident MW power are recorded along with the running time for every microwave activation experiment.

117 Samples were placed in a 60 mm long, quartz reactor, fitted with a sintered disk (0 porosity
118 grade) at its bottom where the biochar rested. The reactor was connected to an adjacent gas
119 manifold using PTFE tubing, from where the gases ($CO_2$ and $N_2$) were fed into the reactor. The
120 flow rate of the gases was controlled using two EL-flow Mass Flow Controllers (MFCs),
121 supplied by Bronkhorst. Gases fed into the microwave reactor vessel exited out of the vessel
122 through the sintered disk located at the bottom of the reactor. These gases would then exit
123 out of the microwave cavity through a vent, which formed part of the built-in exhaust system
124 of the microwave. The exhaust system of the microwave was connected to a laboratory
125 vacuum extractor line.

126 Initial heating tests in the activation apparatus were conducted to ensure that the material
127 could reach the pre-set temperature under MW irradiation. Heating tests were initially
128 performed with the aim of directly replicating the experimental conditions (activation
129 temperature of 600 °C) used to prepare the conventionally-prepared, MCC-based ACs by Biti
130 et al. [11]. Hence, a temperature set point of 600°C, heating rate of 10 °C/min and an inert
131 gas flow rate of 80 NmL/min $N_2$ were all targeted for replication in these experiments. Heating
132 ramp tests of the biochars alone showed that temperature was unable to surpass 300°C,
133 despite the application of the maximum available heating input power from the magnetron,
134 1.8 kW.

135 As a result, a MW susceptor was added in order to improve heating. Commercial AC, Norit
136 R2030CO2 (Norit R), a commercial peat-based AC (2-3 mm particle diameter) supplied by
137 Cabot Corporation, was used as a microwave susceptor for these experiments.

138 With suitable mixing, the addition of a high loss material (Norit R) to a low loss material (MCC
139 biochar) can improve the susceptibility of the low loss material to heat under MW conditions

[19]. With 5 g of biochar, an optimal biochar to susceptor ratio of 1:4 was established for activations. At this ratio, 400 °C was the maximum temperature that could be ramped to and held constantly. Whilst a lower temperature could be potentially limiting to the development of the sorbent during activation, it presents the opportunity to investigate the production an AC under less 'thermally intense' conditions, gauging the effectiveness of microwave heating mechanisms on the material structure.

Before heating, samples were dried to discard the influence of moisture on the MW heating profile of the AC. Both MCC biochars and Norit R were dried in an oven for 16 hours at 100 °C. Mass losses due to drying were found to be in the range of 2-3 wt %. Activation (suffix 'A') of the samples involved their heating at a set heating rate of 10 °C/min from ambient temperature to 400 °C under $N_2$ flow (80 NmL/min). Upon reaching the activation temperature, the gas flow was switched to the activating agent $CO_2$ (20 NmL/min). Activation time was tailored according to target burn-offs, achieved with appropriate residence times for activation. Targeted activation burn-offs were 10 (10 min), 20 (30 min) and 30 wt % (1 hour), which are denoted in sample nomenclature with suffixes 1, 2 and 3, respectively. After activation, the fine-powder, cellulose-based AC produced was separated from the granular Norit R using a stainless-steel sieve (1 mm particle diameter). MCC-derived, MW-prepared ACs were produced and denoted as µC5mA4-1, µC5mA4-2 and µC5mA4-3, with the 'mA4' denoting their MW activation at 400 °C. To re-iterate, activation at a lower temperature allows the opportunity to observe the effectiveness of the MW heating mechanisms and possibly establish a more feasible production process. This in comparison to optimal conventional activation processes which are known to be conducted with activation temperatures of 800-1000 °C in order to produce ACs with maximised performance [11] [20].

## 2.2. Material characterisation

### 2.2.1. Dynamic $CO_2$ Adsorption

The dynamic $CO_2$ adsorption capacity of the ACs was carried out using a Mettler Toledo 3+ Thermogravimetric Analyser (TGA). This was completed based on a procedure from our previous work in order to evaluate the capture potential of these ACs in post-combustion streams where $CO_2$ will be fed in continuous, dynamic flows [11]. The sample (~20 mg) was loaded into a 100 µL aluminium crucible and inserted into the TGA furnace. A pre-treatment step was firstly conducted where the sample was dried by heating at 10 °C/min to 100 °C under $N_2$ flow (50 NmL/min) before cooling to 25 °C. For isothermal capture at 25 °C, the feed gas was switched to $CO_2$ (20 NmL/min) and kept until equilibrium (saturation) was reached. The regeneration stage was completed by a temperature swing where the feed gas was switched back to $N_2$ (50 NmL/min) and temperature raised to 100 °C. The sample was then cooled down to 25 °C and the next adsorption-desorption cycle started. The amount of $CO_2$ adsorbed or desorbed was determined using Equation 1 below [11]:

$$Q_{CO_2} = \left(\frac{m_f - m_i}{m_i}\right) \div M_{CO_2} \qquad \textit{(Eq. 1)}$$

where $Q_{CO_2}$ is the total quantity of $CO_2$ adsorbed (mmol/g), $m_i$ the initial mass of the sample (g), $m_f$ the final mass of the sample (g) and $M_{CO_2}$ the molar mass of $CO_2$ (0.044095 g/mmol) [5]. In the case of adsorption, initial mass ($m_i$) is the mass recorded after pre-treatment/regeneration at 100 °C and the final mass ($m_f$) as the mass at adsorption equilibrium. For desorption, the initial mass is the mass equilibrium prior to its heating and then the final mass is the mass of the sample after regeneration when it has undergone desorption [11]. A total of 10 adsorption-desorption cycles were completed, which in our

185 previous work were deemed suitable for providing an initial assessment of the stability of the
186 material.

187 **2.2.2. Adsorption isotherms**

188 Nitrogen adsorption isotherms measured at -196 °C in a Micrometrics TriStar 3000 analyser
189 have been used for the basis of characterisation of sample textural properties. From the data
190 obtained, the total pore volume was calculated using Gurvich's law, the micropore volume
191 and average pore dimensions were calculated using the Dubinin-Radushklevich (DR) equation
192 and the specific surface area using the Brunauer Emmet Teller (BET) equation [21]. The
193 mesopore volume was calculated as a difference between the micropore volume and the
194 cumulative volume for a pore size of 50 nm, obtained from pore size distribution data [22].
195 Pore size distributions based on $N_2$ isotherm data were determined using DFT model theory,
196 with an assumption of slit-pore geometry.

197 Additionally, $CO_2$ isotherms (measured at various temperatures) were collected using a
198 Micrometrics ASAP 2020 analyser. $CO_2$ isotherms at 0 °C were measured for the
199 determination of the presence of ultra-micropores (< 0.7 nm) [24], which were estimated
200 using the DR equation. Additional $CO_2$ isotherms were collected at 25, 30, 40 and 50 °C to
201 measure $CO_2$ adsorption capacities and to obtain the isosteric heat of adsorption, $Q_{st}$ (kJ/mol)
202 using the Clausius-Clapeyron (Equation 2) [22].

$$-\frac{Q_{st}}{R} = \left(\frac{\partial lnP}{\partial T}\right)_q \qquad \textit{(Eq. 2)}$$

203 where T is the temperature (K), and P is the pressure (Pa) of the gas phase and R the universal
204 gas constant (8.314 J/mol·K).

### 2.2.3. Dielectric properties

The material response to MW radiation is quantifiable through measuring the material's dielectric properties. The dielectric properties of all relevant materials were measured using a 'Dielectric Kit for Vials' purchased from the ITACA , Valencia. The kit consists of quartz vials (8 mL) where sample is placed in a microwave resonator where the properties are measured. For an accurate measurement in this instrument, maximum particle diameters of 2 mm for samples are recommended, hence prior to measuring the dielectric properties of commercial granular AC Norit R, the material was ground to a particle size with the use of pestle and mortar along with a stainless-steel sieve (1 mm). Once the sample was inserted in the vial and a microwave signal generated, the 'resonator probe' shifts its response (resonance frequency and quality factor) depending on the dielectric response of the material. Resultantly, the complex permittivity is measured, thus allowing for the reporting of the dielectric constant, $\varepsilon'$, and the dielectric loss factor, $\varepsilon''$.

The two parameters can be combined into the loss tangent, *tan δ*, which assesses the materials efficiency in converting microwave energy to heat [19]. This is shown in Equation 3 below:

$$tan\delta = \frac{\varepsilon''}{\varepsilon'} \qquad \textit{(Eq. 3)}$$

The dielectric properties of samples for these experiments were measured at room temperature (~25 °C) with a frequency of 2.45 GHz.

### 2.2.4. Elemental Analysis

Samples were subjected to elemental analysis to determine C, H, N and O content. Before analysis, samples were oven-dried at 70 °C for approximately two weeks. The analysis itself was conducted using a Thermo Scientific FlashSmart analyser at the University of Birmingham, UK.

### 2.2.5. Point of Zero Charge

The surface acidity/basicity of ACs was characterised by measuring the point of zero charge ($pH_{PZC}$), the pH at which the surface charge is neutral [23]. This was determined by a mass titration procedure adopted from Noh and Schwarz [24]. Approximately 0.250 g of AC sample was placed and sealed in a tube where it was suspended in distilled water. The remaining open space between the suspension and the tube was filled with $N_2$ to maintain an inert atmosphere within the tube, and the suspension stirred continuously at room temperature using a magnetic stirrer. Each day prior to adjusting mass concentration, the pH of the suspended samples was measured once equilibrium was reached. After daily measurements, an increment of distilled water was added to the tube, reducing the proportion of sample mass in the suspension. This procedure was carried out over a 10-day period before the $pH_{PZC}$ was determined as an average of the most consistent range of pH values measured for each sample.

### 2.2.6. FTIR Spectroscopy

The chemical structure of the ACs produced was also characterised by FTIR spectroscopy using a Perkin-Elmer Spectrum Two FT-IR Spectrometer fitted with an attenuated total reflectance accessory. Spectra were collected across a wavenumber range of 450-4000 $cm^{-1}$, using a scan resolution of 4 $cm^{-1}$ and two scans per sample.

### 2.2.7. Thermal Stability Analysis

The thermal stability of the ACs was assessed using The Mettler Toledo 3+ TGA instrument. Approximately 20 mg of sample was placed in an aluminium oxide crucible and inserted into the TGA furnace. Samples were subjected to a heating ramp (10 °C/min) across a temperature range of 25-1000 °C under $N_2$ flow (50 NmL/min). The mass (wt %) was recorded with increasing temperature, thus identifying associated mass losses from which an assessment of the material thermal stability could be made.

## 3. Results and discussion

### 3.1. Dynamic adsorption-desorption cycles

The 10-cycle $CO_2$ adsorption-desorption profiles for the MW-prepared ACs are depicted in Figure 1 along with the profile of Norit R. The temperature profile is also added to indicate the stages of adsorption (25 °C) and desorption (100 °C) more clearly. All the MW-prepared ACs show a robust, stable capture capacity across the 10 cycles, with minimal fluctuations (± 2 %). The clearest trend in the profiles is the increase of $CO_2$ adsorption capacity (average and total) with increasing activation burn-off. AC µC5mA4-1, the AC subjected to the least extent of activation, possesses the lowest $CO_2$ adsorption capacity (Average: 1.47 mmol/g) whilst larger cyclic $CO_2$ adsorption capacities are observed for ACs µC5mA4-2 (Average: 1.64 mmol/g) and µC5mA4-3 (Average: 1.73 mmol/g). Also notably, ACs µC5mA4-2 and µC5mA4-3 possess larger $CO_2$ adsorption capacities than commercial AC Norit R (Average: 1.58 mmol/g). This indicates that the MW activation procedure applied is effective in enhancing the $CO_2$ adsorption capacity, even at the moderate temperature and burn-off conditions applied.

Whilst all ACs including Norit R show suitable desorption performance under the conditions tested, desorption, particularly in a TSA, will pose a greater challenge at larger scales. Particularly with the use of a sweeping gas, there is the possibility of largely 'diluted' streams of $CO_2$ being produced, which is not desirable particularly for the storage and transport of $CO_2$ [11]. As has been explored with Norit R at larger experimental scales, there exist adjusting desorption parameters such as reduced sweeping gas flow rate [25]. Nonetheless, this study presents the production of ACs with very quick activation durations (10 min - 1 hour), that display superior (µC5mA4-3, µC5mA4-2) or similar (µC5mA4-1) $CO_2$ capture capability compared to a commercial AC developed for $CO_2$ capture (Norit R).

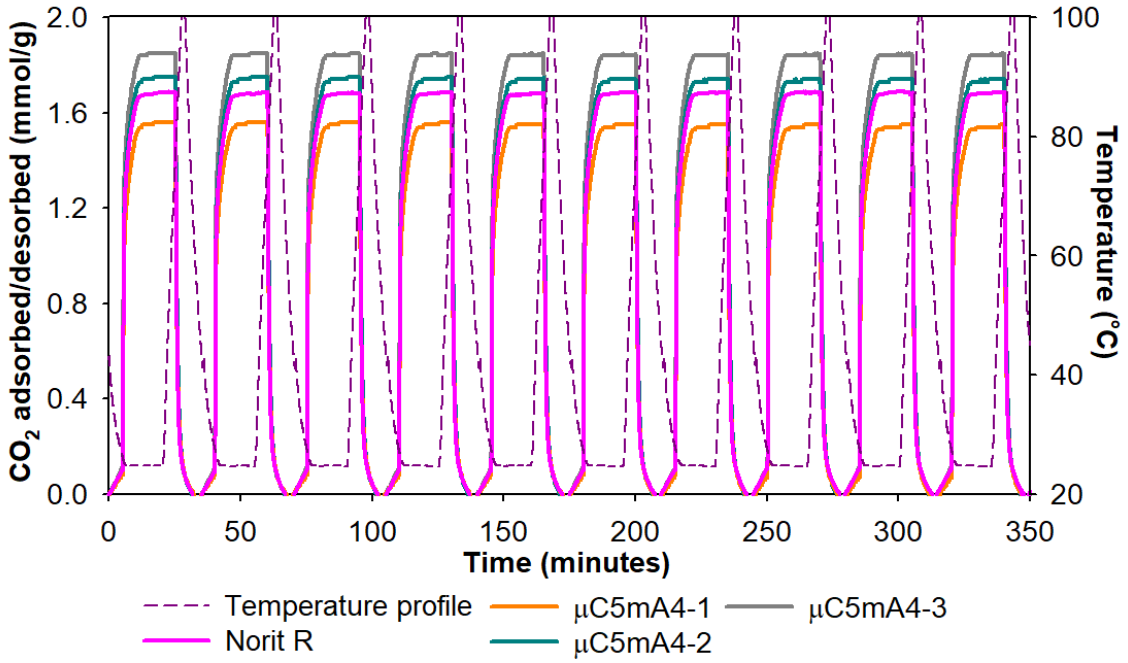


**Figure 1:** MCC sorbents 10-Cycle $CO_2$ TGA adsorption/desorption profiles

### 3.2. Supporting characterisation

#### 3.2.1. Adsorption isotherms and Textural properties

Adsorption, the transfer of a specific component from its fluid phase to the surface of a solid, is the primary mechanism to which $CO_2$ is captured by these sorbents [26]. More specifically,

these sorbents adsorb $CO_2$ through the mechanism of physisorption, where the diffused molecules are affixed to the walls of the pores of the sorbent, primarily through Van der Waals forces [9]. Thus, through physisorption, adsorption isotherms for both $CO_2$ and $N_2$ are generated where details regarding adsorption capacities ($CO_2$) or textural properties ($CO_2$ and $N_2$) can be obtained.

The $N_2$ and $CO_2$ adsorption isotherms produced for these sorbents are available in the Supplementary Information. The textural properties from adsorption isotherm data for these ACs are summarised in Table 1. Also added are ACs from our previous work that will be elaborated on further in Section 3.3. The mainly microporous structure of these MW-prepared ACs is confirmed by their calculated textural properties, where pore volumes indicate that these ACs possess a high degree of microporosity ($W_0/W_T > 0.90$). Average pore sizes obtained also confirm that the pores present in these ACs are generally microporous whilst the BET surface areas of the ACs are relatively moderate ($S_{BET}$: 375-510 $m^2/g$). Across the varying activation treatments, the most notable changes are the increase in $S_{BET}$ and pore volumes ($W_T$ and $W_0$) with increasing burn-off, whilst average micropore width, $L_0$, decreases with increasing activation burn-off. This is indicative of textural property development under MW heating and them being promoted further by increasing the duration of the treatment. Textural property calculations from $CO_2$ isotherms at 0 °C reveal that average ultramicropore width ($L_{0,ultra}$) was at its highest at 10 wt % burn-off, whilst longer activation times gave smaller values of $L_{0,ultra}$ at 20 and 30 wt %, although both these samples were similar to each other. Ultramicropore volume, $W_{0,ultra}$, is at its largest at 10 wt % burn-off before reducing and remaining consistent at burn-offs of 20 and 30 wt %. These observations indicate that whilst MW activation with $CO_2$ is effective in generating microporosity, this is only to a certain extent determined by the burn-off condition. Beyond a certain degree of activation burn-off (20 wt

%), the generation and development of new, narrow micropores is not guaranteed. Overall, the most pronounced changes in textural properties with increasing activation burn-off include in BET surface area, total and micropore volume, as well as the narrowing of the average micropore and ultramicropore widths. These changes are also key contributors to changes in $CO_2$ adsorption capacity amongst the varying activation burn-offs.

Whilst increased development of the textural properties could perhaps be expected for ACs at higher activation burn-offs, it is particularly promising that notable changes in the development of the AC textural properties can be achieved at the considerably reduced activation temperature used, 400 °C.

**Table 1:** Textural properties of conventionally-prepared and MW-prepared ACs obtained from adsorption isotherms: $N_2$ at -196 °C (a-e) and $CO_2$ at 0 °C (f-g)

| Sample | $S_{BET}$ [a] ($m^2/g$) | $W_T$ [b] ($cm^3/g$) | $W_0$ [c] ($cm^3/g$) | D[d] (nm) | $L_0$[e] (nm) | $W_{0,ultra}$[f] ($cm^3/g$) | $L_{0,ultra}$[g] (nm) | Ref. |
|---|---|---|---|---|---|---|---|---|
| µC5mA4-1 | 375 | 0.16 | 0.15 | 1.77 | 1.01 | 0.27 | 0.73 | This study |
| µC5mA4-2 | 434 | 0.21 | 0.20 | 1.75 | 0.84 | 0.25 | 0.60 | |
| µC5mA4-3 | 510 | 0.23 | 0.21 | 1.80 | 0.72 | 0.25 | 0.59 | |
| µC5A6-1 | 434 | 0.19 | 0.18 | 1.78 | 0.94 | 0.21 | 0.62 | [6] [11] |
| µC5A6-2 | 443 | 0.20 | 0.19 | 1.80 | 0.72 | 0.23 | 0.62 | |
| µC5A6-3 | 487 | 0.21 | 0.20 | 1.72 | 0.63 | 0.27 | 0.59 | |
| Norit R | 870 | 0.62 | 0.37 | 2.84 | 1.41 | 0.26 | 0.64 | This study |

*[a]BET surface area; [b] Total pore volume; [c] Total micropore volume; [d]Average pore diameter; [e]Average micropore width; [f]Ultramicropore volume; [g]Average ultramicropore width*

### 3.2.2. Static and dynamic $CO_2$ adsorption behaviour at 25°C

In line with observations under dynamic adsorption conditions, $CO_2$ adsorption capacity under static conditions also increases with increasing activation burn-off. Quite apparent is that $CO_2$ adsorption capacities measured under TGA dynamic conditions are generally lower than those measured at equilibrium conditions using $CO_2$ isotherms (static conditions) at 25 °C (2.32-2.43 mmol/g). One of the main reasons for this lower retention of $CO_2$ on the sorbent

surface is the increased mobility of $CO_2$ under dynamic conditions [27] [28]. The changes in $CO_2$ adsorption capacity at 25 °C with increasing burn-off is also more pronounced under dynamic conditions compared to those observed under static conditions. This is particularly evident when assessing the $CO_2$ adsorption capacities between ACs µC5mA4-1 and µC5AmA4-2. Whilst their differences in $CO_2$ adsorption capacity under equilibrium conditions were more marginal (~0.02 mmol/g), their difference according to average single cycle adsorption capacities is 0.19 mmol/g. This is indicative of the variations in textural properties likely being more influential under dynamic conditions, particularly the narrowing of micropore widths ($L_0$ and $L_{0,ultra}$), as well as the increase in pore volumes ($W_T$ and $W_0$), with increasing activation burn-off.

Under equilibrium conditions, rather unique is the $CO_2$ adsorption behaviour of µC5mA4-1. Despite having notably lower $S_{BET}$ and $W_0$, it still possesses a substantial $CO_2$ adsorption capacity (2.32 mmol/g) of close magnitude to µC5mA4-2 (2.34 mmol/g) and µC5mA4-3 (2.43 mmol/g). Its more notable $CO_2$ adsorption capacity could be accounted for by its possessing of the largest ultramicropore volume ($W_{0,ultra}$ = 0.27 $cm^3/g$) and wider average ultramicropore width ($L_0$ = 0.73 nm). Under dynamic adsorption conditions, the changing textural properties, specifically pore volumes and average micropore size ($L_0$) are thus more influential at least at burn-offs above 10 wt %.

The static adsorption capacities of these MW-prepared ACs are smaller than that of Norit R (2.62 mmol/g), yet the MW-prepared ACs µC5mA4-2 and µC5mA4-3 were found to possess higher $CO_2$ adsorption capacities under dynamic conditions. The measured $CO_2$ adsorption capacities at equilibrium of commercial AC Norit R are also included in supplementary information. Norit R, whilst possessing similar PSD to the MW-prepared ACs (1.5 nm ≤ PSD <

160 nm), possesses larger key textural properties ($S_{BET}$ = 870 $m^2/g$; $W_T$ = 0.62 $cm^3/g$; $W_0$ = 0.37 $cm^3/g$) that contribute to its greater equilibrium adsorption capacity. However, its lower degree of microporosity ($W_0/W_T \approx 0.60$) and wider pore dimensions ($L_0$ = 1.41 nm; D = 2.84 nm) appears to limit its dynamic adsorption capacity under the dynamic conditions tested. The presence of narrow micropores improve the adsorbent-adsorbate interactions, and thus the adsorption capacity, whilst wider pores may be beneficial for channelling $CO_2$ molecules to narrower pore structures. Thus, it is strongly likely that Norit R, based on the nature of its textural properties, also displays an adsorption performance that is influenced by its textural properties when compared to the MW-prepared ACs. Also, to be considered is that Norit R is in granular form, which may be less favourable than the powder form due to greater limitations in the $CO_2$ diffusion compared to the powder form at the TGA experiment measured using little quantities of sample. Whilst the dynamic conditions tested are not optimally designed for $CO_2$ capture, the MW-prepared ACs do appear to possess textural characteristics that would be promising for industrial applications. The textural properties of these MW-prepared ACs were also achieved under milder activation burn-off conditions (10-30 wt %). For dynamic $CO_2$ adsorption under the conditions used (25 °C, 101.3 kPa), it has been noted that the parameter that influences $CO_2$ adsorption the most is the volume of narrower pore sizes that are predominantly in the ultramicropore size range < 1 nm [29] [30].

Considering the observed narrowing of $L_{0,ultra}$ with increasing activation burn-off, there also lies the opportunity to produce MW-prepared ACs at higher activation burn-off that will likely possess narrower pore sizes and perhaps larger pore volumes (total and micro), resultantly leading to higher $CO_2$ adsorption capacities.

### 3.2.3. Elemental analysis and Point of Zero Charge

Table 2 depicts the elemental composition and $pH_{PZC}$ for MW-prepared ACs along with raw MCC and the parent biochar used µC5 [11]. Evidently, highly carbonaceous ACs (C content > 87 wt %) are produced, with more pronounced changes during conversion of MCC to biochar. Smaller changes are still observable as C content increases as the biochar is activated . The transformation of MCC from raw feedstock to biochar and AC form is conveyed further through the observed reductions in oxygen (O) and hydrogen (H) content that occur due to the decomposition and aromatisation reactions taking place during the treatment. In addition to the observed changes in $CO_2$ adsorption capacity of the ACs, these chemical compositional changes further indicate that the use of moderate/low activation temperature is still effective for material development by MW-assisted activation.

A notable and perhaps peculiar finding is the presence of nitrogen (N) in ACs µC5mA4-2 and µC5mA4-3. This may have occurred as a result of a combination of the nitrogenous atmosphere formed inside the reactor during the heat ramp along with micro plasma hot spots that can emerge during MW heating. ACs µC5mA4-2 and µC5mA4-3 are subjected to prolonged duration of MW activation compared to AC µC5mA4-1 and are thus more susceptible to the influence of micro plasma hotspots, which in this instance results in the apparent introduction of N into the AC structure. The incorporation of N under these conditions was also observed by Tsyganov et al., who assessed the introduction of small

quantities of N into graphene structures through MW heating (2.45 GHz, 2 kW) under $N_2$ flow at atmospheric conditions [31]. In their findings they established that whilst $N_2$ itself will not directly dissociate under plasma conditions due to its good stability, carbon-nitrogen radical species may form through reactions of $N_2$ with radical carbon species from the carbonaceous/graphitic material, along with any C available in gaseous form [31]. These mechanisms are described by the following Reactions 1.1-1.6 [31]:

$$CN^{\bullet} + H_2 \rightarrow HCN + H \qquad (R.\ 1.1)$$

$$N_2 + CH_2 \rightarrow H_2CN + N \qquad (R.\ 1.2)$$

$$N_2 + CH \rightarrow HCN + N \qquad (R.\ 1.3)$$

The formation of a CN radical, $CN^{\bullet}$, leading to the formation of HCN, is also possible through the following mechanisms [31]:

$$N_2 + C \rightarrow CN^{\bullet} + N \qquad (R.\ 1.4)$$

$$C_2 + N_2 \rightarrow CN^{\bullet} + CN \qquad (R.\ 1.5)$$

The emergent HCN is assumed to form in the N graphene structure of the carbonaceous materials in the following fashion:

$$C(s) + HCN \rightarrow \text{N-graphene} + 0.5\ H_2\ (g) \qquad (R.\ 1.6)$$

Whilst originally unintended, the introduction of N into the structures of ACs µC5mA4-2 and µC5mA4-3 is welcomed. The incorporation of N into the structures of AC has been explored extensively in studies as a mean to improve the surface basicity of ACs and enhance the $CO_2$ capture capacity [32]. This is achieved through the N in the structure being able to share its lone pair with $CO_2$, a weak acid that will accept the lone pair [7]. Another mechanism that has been proposed is the doped N-atom promoting hydrogen bonding between oxygen from the $CO_2$ molecule and hydrogen in C-H or N-H groups within the AC structure [33]. N-doping

405 treatments have been explored extensively in studies to introduce N into the carbonaceous
406 structure of the AC and thus improve the $CO_2$ capture capacity. Typical N-doping procedures
407 require an N-doping precursor which can be incorporated into the AC by various treatment
408 methods, including wet impregnation or thermal treatment [7]. The resultant incorporation
409 of N into the ACs described in this work is particularly advantageous as it did not require an
410 additional experimental step.

411 Measurements of $pH_{,PZC}$ show that these MW-activated ACs do possess basic surface
412 character ($pH_{,PZC} > 7$) with the basicity slightly increasing with increasing in activation burn-
413 off. Whilst the increase in surface basicity observed with an increase in O content and a
414 decrease in H content may also correspond to more basic surface functionalities forming from
415 10 to 30 wt % burn-off, the addition of N content to the ACs also likely contributes to the
416 higher degree of basicity. This as a result of the doped N, incorporated into the structure of
417 the AC most likely in pyridinic or pyrrolic configuration, possessing Lewis base functionality
418 and thus promoting surface basicity [7]. For AC µC5mA4-1, which does not possess any N
419 content, yet possess larger $pH_{,PZC}$ than µC5, MW heating itself may have contributed to
420 altering surface functionalities. This through the biochar perhaps heating more uniformLy
421 under MW conditions compared to conventional conditions, or even the presence of MW
422 hots pots, may have allowed more extensive removal of surface acidic groups from the
423 sorbent surface in the form of CO or $CO_2$ [7]. The reduction in O content from biochar form
424 to activation at 10 wt % burn-off (µC5mA4-1) is also indicative of this behaviour. In addition,
425 $pH_{,PZC}$ show that µC5mA4-1 ($pH_{,PZC}$ = 8.24) does possess similar surface basicity to the ACs
426 such as µC5mA4-2 ($pH_{,PZC}$ = 8.57), according to which may have aided its $CO_2$ adsorbing

capability despite its predominantly less developed textural properties and not possessing any N content that may have promoted $CO_2$ adsorption.

In light of the desirability of surface basicity to improve $CO_2$ affinity to the AC surface, the observed increase in $pH_{,PZC}$ with increasing burn-off is a likely contributor to the improved $CO_2$ adsorption capacity with increased burn-off that is observed for these MW-prepared ACs. Like the observed influence of pore volumes and micropore sizes, the influence of surface basicity is more pronounced under dynamic than static conditions.

**Table 2:** Sample elemental composition (wt%) & Point of Zero charge

| Sample | C | H | N | O | $pH_{,PZC}$ |
|---|---|---|---|---|---|
| Raw MCC | 42.20 | 6.35 | 0.00 | 51.46 | - |
| µC5 | 85.03 | 3.04 | 0.00 | 11.94 | 7.22 |
| µC5mA4-1 | 90.30 | 1.09 | 0.00 | 8.62 | 8.24 |
| µC5mA4-2 | 90.49 | 0.65 | 0.15 | 8.72 | 8.57 |
| µC5mA4-3 | 87.54 | 0.46 | 0.08 | 11.94 | 8.72 |

### 3.2.4. Materials dielectric response

Table 3 details the dielectric properties of both raw MCC and its biochar µC5. Biochar loss tangent values are at the lower limit of the ideal range for MW heating applications ($0.01 < tan\delta < 5$) [34], with no enhancement of the dielectric properties after carbonisation as the biochar presents smaller loss tangent (*tanδ)* value compared to the original cellulose feedstock. The reduced dielectric properties can be attributed to the decrease in resultant density of the material [35]. During carbonisation of the raw MCC to produce biochar, approximately 75 wt % of the original MCC is decomposed [11], leading to a reduction in the number of atoms per unit volume, and thus less available atoms for polarisation [35]. In addition, there may exist insulating barriers between particles that would inhibit interfacial polarisation [35]. Regarding the thermal degradation of raw MCC during pyrolysis, the greater thermal degradation occurs primarily in a temperature range of 300-400 °C, with the

446 breakdown of the structure through dehydration and depolymerisation expected to occur
447 alongside biochar formation mechanisms such as aromatisation [36]. Considering the
448 relatively mild carbonisation temperature used to produce the biochar (500 °C) [11], the
449 structures of the cellulosic biochar produced correspond to early-stage biochar formation
450 through cellulose pyrolysis. Biochars with greater dielectric properties are typically those
451 produced at elevated temperatures, where a higher degree of formation of the carbonaceous
452 structure has occurred and insulation barriers amongst particles in the biochar are removed,
453 thus promoting interfacial polarisation effects [35] [13]. Therefore, with a lack of
454 development of the carbonised structure, the conductivities of these cellulosic-based biochar
455 is limited, thus accounting for the modest dielectric properties observed. Other studies have
456 noted a typical increase in the conductivity of pyrolysed cellulose at elevated temperatures,
457 particularly above the 500 °C carbonisation temperature used here [37] [38]. For example,
458 Rhim et al. found biochar from pyrolysed microcrystalline cellulose to begin to show
459 considerable increase in conductivity from a carbonisation temperature range of 550-600 °C,
460 with a five-order of magnitude increase in the conductivity observed in the temperature
461 region of 610-1000 °C, due to the formation of a more graphitic carbon structure [38]. Also
462 recorded in Table 3 are the dielectric properties of the activated carbon Norit R, a presumably
463 more 'graphitised' sorbent compared to the biochar. Thus expectedly, it possesses a superior
464 dielectric response compared to the cellulose-derived biochar, which justifies its use as a
465 susceptor to improve the heating of the MCC-based biochars.

**Table 3:** Dielectric properties of cellulose feedstock, biochar and commercial activated carbon Norit R as potential MW susceptor, measured at 25 °C

| Material | $\varepsilon'$ | $\varepsilon''$ | $tan\delta$ |
|---|---|---|---|
| Norit R | 16.47 | 9.38 | 0.57 |
| MCC (μ) | 1.50 | 0.09 | 0.05 |
| μC5 | 1.41 | 0.01 | 0.01 |

Further characterisation of the ACs pertaining to their physical, chemical and adsorptive properties are available in the supplementary information. This includes FTIR spectroscopy, TGA thermal stability, heat of adsorption and selectivity data.

### 3.3. Comparative analysis of MW vs conventionally prepared ACs

#### 3.3.1. $CO_2$ capture under equilibrium and dynamic conditions

The ACs produced in this study have been compared to ACs from a previous work, developed via conventional activation means, where activation took place in a tubular furnace at 600 °C [11]. The heating rate, both the inert and activation gases flow rates were all kept identical. Thus, AC samples μC5A6-1, μC5A6-2 and μC5A6-3 correspond to the ACs with 10, 20 and 30 wt % burn-off [11]. This section compares these ACs, considering that the MW-prepared ACs produced in this work were activated at a 200 °C lower temperature, from which an assessment of the effectiveness of the MW activation procedure can be made.

The textural properties of the conventionally and MW prepared ACs are displayed in Table 1. Both series of ACs present relatively moderate BET surface areas (375-510 $m^2/g$) and high degree of microporosity ($W_0/W_T$ > 0.90). Overall, the MW-prepared ACs, despite being produced at 200 °C lower temperature and with 83-94 % shorter durations to achieve the targeted burn-offs (see Table 4), possess textural properties of similar, comparable nature to conventionally prepared ACs.

Figure 2 depicts the maximum $CO_2$ adsorption capacities for the ACs under equilibrium conditions (volumetric measurement, using a Micrometrics ASAP 2020 analyser), as well as the average single cycle dynamic $CO_2$ adsorption capacities (measured by TGA). Regarding the maximum adsorption capacities at equilibrium, all MW-prepared ACs possess higher $CO_2$ adsorption capacities (2.32-2.43 mmol/g) than the conventionally prepared ACs (1.82-2.28 mmol/g). This, despite conventionally prepared ACs possessing narrower average micropore widths. Since the other textural parameters among the two series are of similar values, a key distinctive aspect here may be the surface character of the materials, according to their point of zero charge, $pH_{,PZC}$. Measurements of $pH_{,PZC}$ show that the MW-activated ACs possess more basic surface character ($8.20 < pH_{,PZC} < 8.80$) than the conventionally prepared ACs ($6.90 < pH_{,PZC} < 7.90$) [11]. For ACs μC5mA4-2 and μC5mA4-3, the introduction of nitrogen may have contributed to their surface basicity. Also, to be considered is the more basic character of nitrogen-deficient AC μC5mA4-1 ($pH_{,PZC} = 8.24$), compared to conventionally- prepared AC μC5A6-1 ($pH_{,PZC} = 7.18$) which also does not contain any N. This is indicative of MW heating being more effective than conventional heating in establishing more basic surface character in the AC with the chemical changes achieved, which included reductions in H and O content from its original biochar form (μC5). This, through the alternate heating profile generated by interfacial polarisation effects and hot spot formation during activation. MW heating mechanisms will tend to heat solid materials that consists of the transfer of heat from the interior of the material to the surface, unlike in conventional heating where heat transfers from the surface to the interior of the material [39].

Overall, a combination of the textural properties and the changes in chemical composition that promoted basic surface character that were achieved with MW heating appear as the

main drivers of the improved performance of these MW-prepared ACs, compared to the conventionally-prepared ACs.

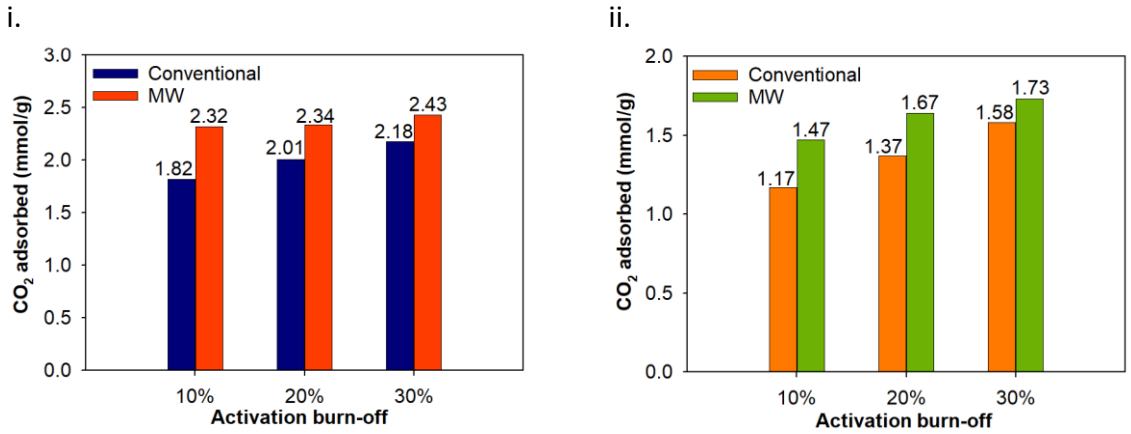


**Figure 2:** $CO_2$ adsorption capacities for conventional and MW-prepared ACs at 25 °C, 101.3 kPa under i. Static conditions ii. Dynamic conditions (average single cycle, (standard deviation σ = ± 0.01)

510 The $CO_2$ capture capacities exhibited by the MCC-based sorbents prepared using conventional
511 heating were exhaustively compared with the capacities shown by similar materials produced
512 using a wide range of lignocellulosic feedstocks in our previous work [11]. It was concluded
513 that, expectedly, the largest $CO_2$ adsorption capacities were observed from ACs produced by
514 chemical activation. For example, the outstanding capacities exhibited by the KOH-activated
515 water chestnut shell, and pine saw dust: 4.54 and 4.21 mmol/g at 25°C, respectively [27] [40].
516 However, the ACs produced by chemical activation are a less environmentally favourable
517 option at larger scale compared to physically activated ACs. In the opposite side of the ranking
518 in terms of $CO_2$ adsorption performance are some of the lignocellulosic materials reported in
519 literature. For instance, raw bamboo activated with phosphoric acid (1.45 mmol/g at 25°C
520 [41]), palm kernel shell AC physically activated with $CO_2$ (2.13 mmol/g at 25°C [41]),
521 commercial granular AC (1.89 mmol/g at 25°C, [42]), and steam-activated NoritRSX2 (1.88
522 mmol/g at 25°C [41]) were found to achieve greatly smaller $CO_2$ adsorption capacities than
523 the exhibited by the materials produced from MCC, and specially the prepared in this work
524 using microwave heating for activation.

525 **3.3.2. Energy consumption during microwave activation**

526 In addition to assessing AC physicochemical properties and the $CO_2$ capture capacities, a key
527 comparison between conventional and MW heating is the energy consumption of the two
528 methods. More specifically, the energy consumption during activation was assessed since
529 both AC types underwent the same carbonisation process [6]. For both apparatuses, the
530 energy consumption (kWh) during activation was calculated by trapezoidal integration of the
531 area under the curve of power against time recorded. The formula is depicted in Equation 4
532 as follows:

$$E = \sum(t_i - t_{i-1}) \left( \frac{P_i + P_{i+1}}{2} \right) \quad \textit{(Eq. 4)}$$

where E is the energy consumption (kWh), P is the power input (kW), and t is the time (h).

Figure 3 depicts the power input profiles during activation (heat ramp + isothermal heating), using conventional (furnace) and MW heating for the prepared ACs. In the case of both heating sources, the largest power inputs are recorded at the end of the heating ramp to the isothermal activation temperature (furnace: 0.98 hours, MW: 0.63 hours, respectively). Fluctuations in power input are generally observed for both the furnace and the microwave across the activation duration. This is due to the prolonged isothermal heating step, characteristic of the activation stage which commences once the gas is switched to $CO_2$ at the isothermal activation temperature. However, the power input applied by the furnace fluctuates in a lower power range (0.10-0.35 kW) compared to the power input applied by the MW magnetron (0.25-0.90 kW) in this isothermal region. The obtained profiles do clearly demonstrate the more advantageous heating mechanisms associated with MW heating. Whilst conventionally-prepared ACs require activation durations in the order of several hours, MW-activations were completed in the order of minutes. The most extensive activation burn-off condition, 30 wt %, is achieved within 1 hour duration (isothermal step) with MW heating, which corresponds to only the 6.3 % of the time required to achieve the same burn-off through conventional heating.

Table 4 details the duration and total energy consumption for the thermal activation process using both conventional and MW heating. The substantially lower activation durations used in the MW-approach translates into reduced energy consumptions, with MW consuming 52 % less energy at 10 wt % burn-off condition, 39 % less at 20 wt % and 68 % less at 30 wt % burn-off.

Whilst it cannot be ignored that activation procedures in the tubular furnace are conducted at 200 °C higher temperatures than in the microwave which may warrant increased power input, substantially longer activation durations are still required to achieve the desired burn-off in the furnace. Hence in terms of the heating intensity (temperature and duration) required for the development of the ACs, MW-heating proves to be much more effective. It is also evident that Norit R, a commercially available, cheap, easily accessible, and separatable susceptor, has performed effectively enough to foster the development of these promising ACs under less intense production route.

To be emphasised, however, is that the energy consumption presented only represents the consumption used by the apparatus' respective heating elements, not necessarily the full apparatus. For instance, MW radiation generated at frequency 2.45 GHz is done so typically with 50 % efficiency from the electrical energy used [39]. Further assessment of the process efficiency, particularly for feasible process scale-up, would require factoring in the input of electrical energy for the microwave along with additional energy consumption from supplementary components (e.g. digital systems and controllers), through assessing consumption from mains plug connections.

| Conventional | Microwave |
|---|---|
| 10 wt % burn-off | |

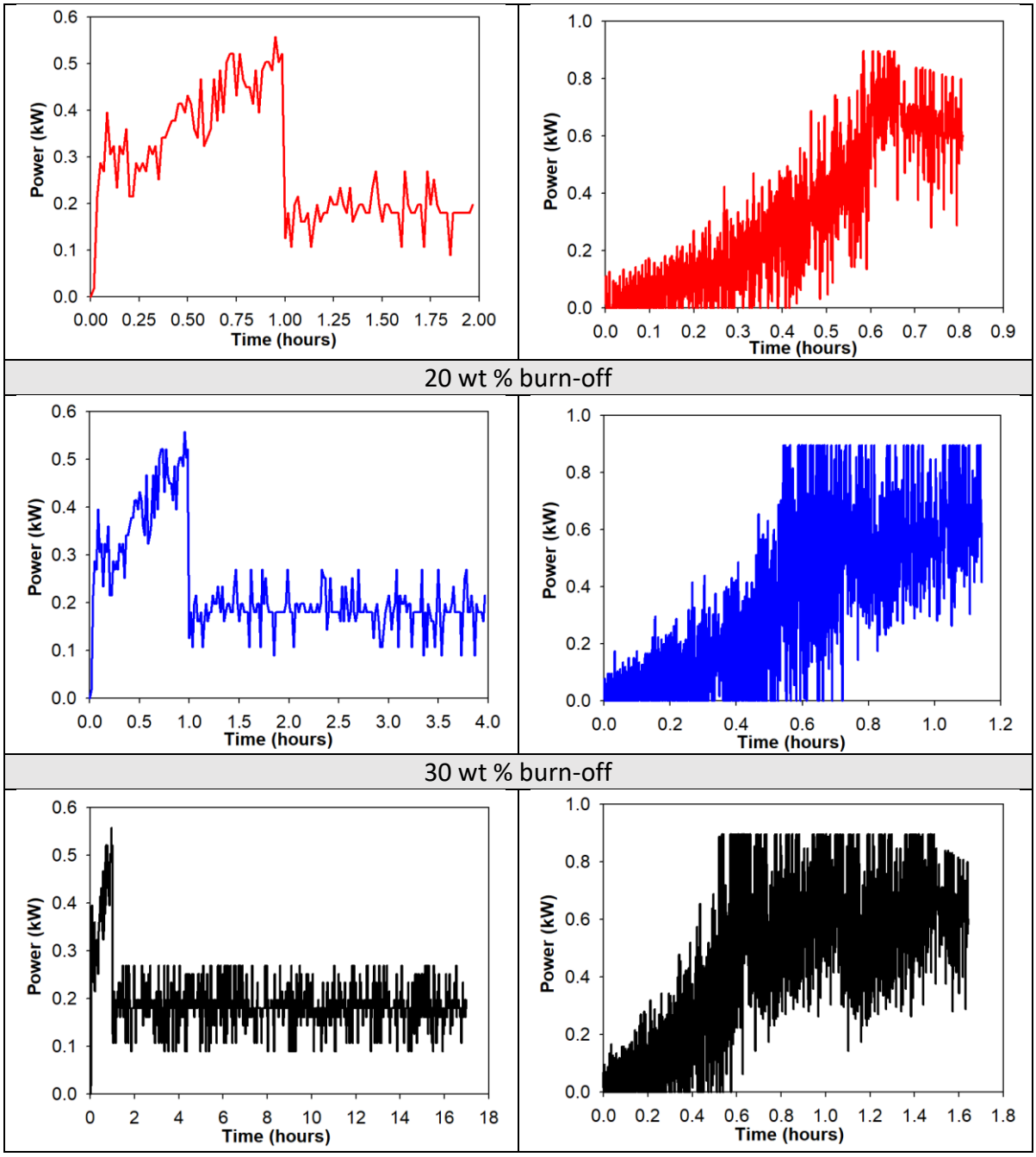


**Figure 3:** Activation power input profile for conventionally- and MW-prepared ACs

574

**Table 4:** Energy consumption summary for conventional and MW activations

| Activation Mode | Duration (h) | Energy consumption (kWh) | Reference |
|---|---|---|---|
| 10 % burn-off | | | |
| Conventional | 1 | 0.56 | [11] |
| MW | 0.17 | 0.27 | This study |
| 20 % burn-off | | | |
| Conventional | 3 | 0.92 | [11] |
| MW | 0.33 | 0.56 | This study |

| 30 % burn-off | | | |
|---|---|---|---|
| Conventional | 16 | 3.31 | [11] |
| MW | 1 | 1.06 | This study |

575

576 **3.5. Discussion**

577 The findings from this study have represent a promising developmental pathway for a
578 'greener' carbon capture that can be implemented into $CO_2$ emitting industries. 'Greener' in
579 terms of the environmentally friendliness associated using MCC, a feedstock available from a
580 wide array of waste sources, as previously stated. This, without the use of environmentally
581 harmful chemical activating agents during AC preparation. Added to this is the producing of
582 suitable ACs more efficiently, as highlighted by the considerably milder activation
583 temperature and shorter activation times. The comparison made with conventional activation
584 also shows that there is a significant opportunity to optimise the production of ACs efficiently
585 using MW heating. As shown from the development of the textural properties, higher
586 activation burn-offs will generally promote improved textural properties that are suitable for
587 $CO_2$ adsorption. In this study, MW heating has demonstrated a greater capability to maintain
588 a suitable degree of efficiency when increasing the activation burn-off. This is evident with
589 the 83-94 % shorter activation times and 39-68 % lower power input achieved when
590 compared to conventional processes. To be considered however is that in activating to higher
591 activation burn-offs and temperatures, the increased 'thermal intensity' will test material
592 stability more broadly and deeply, hence the favourable material development to maximise
593 $CO_2$ capture may or may not necessarily be guaranteed. Thus, activations to higher burn-offs
594 and with higher temperatures will allow for the determining of more conclusive burn-off and
595 temperature thresholds for optimal AC development and $CO_2$ capturing ability also with
596 respect to energy consumption.

A key limit encountered experimentally in this study was the heating of the cellulosic biochars during activation being restricted by the biochars' dielectric response. This resulted in the use of a MW susceptor which could only achieve stable heating at up to 400 °C. There exists various other carbon-based susceptors from literature with reportedly better dielectric properties than Norit R (*tanδ* = 0.57) that could be used to increase the activation temperature of the cellulosic biochars based on their dielectric properties. This includes carbon black (*tanδ* = 0.83), carbon nanotubes (*tanδ* = 1.14), and silica carbide (*tanδ* = 0.58-1.00) [43] [49]. Considering the very similar dielectric response between raw MCC and biochar µC5, process efficiency may be simplified by incorporating susceptors into the carbonisation stage or establishing a one stage carbonisation-activation procedure as has been reported in other studies [12]. However, the performance of MW-prepared ACs from literature has indicated that a separate carbonisation step is beneficial for maximising AC development. This was demonstrated by Durán-Jiménez et al. who produced KOH-activated carbon with higher $CO_2$ adsorption capacity using a two-step production as opposed to a single activation step, which allowed for the greater development of textural properties [12].

Also evident was an apparent form of N-doping into the AC structure most likely due to micro plasma hotspots formation. Activation at higher burn-off conditions and temperature will be beneficial to further investigate this occurrence, possibly of N-doping that is at least less process-intensive compared to typical N-doping procedures which may require an additional experimental step in the AC preparation process. Micro plasma hot spots are typically undesirable for heating uniformity and the quality of the heating process of the material [34]. However, the MW-prepared ACs produced in this study exhibit textural property development similar to conventionally-prepared ACs, despite the former being produced at a

200°C lower a temperature. This is indicative of the heating profile produced during heating, whilst perhaps not completely and consistently uniform, still proving effective enough for textural property development and changes in the chemical structure (C,H,N,O, $pH_{PZC}$). Conducting activation procedures at higher temperatures should also be beneficial in further establishing the suitability of this heating profile, and the extent of N-doping effects.

Whilst findings from dynamic adsorption-desorption tests proved promising, they also emphasise the importance of measuring $CO_2$ adsorption capacities not just under static conditions. As mentioned previously, the TGA is not an apparatus designed primarily and optimally for $CO_2$ capture. Thus, further experimental scope also certainly exists for expanding on this initial assessment of these ACs' dynamic adsorption potential. This includes not only testing with larger quantities of AC at larger experimental scales (thermal swing adsorption system), but also establishing optimal adsorption parameters and an optimal bed configuration for TSA regeneration (fixed, fluidised, rotary beds) [44]. In addition, this includes a configuration that best complements the powder form of these ACs, otherwise AC pelletisation processes that minimise any hinderances of the AC performance will require consideration [45].

The robust material stability shows promise and justification for their testing beyond 10 adsorption-desorption cycles. In applying extended TSA cycles, particularly at larger scales, the energy efficiency for regeneration will be more prominent in assessing the overall feasibility. In light of having used MW heating to improve the production efficiency as has been demonstrated, a means to improve the efficiency of desorption can be through microwave swing adsorption (MWSA), which has also been explored as a promising means of sorbent regeneration compared to conventional TSA [25] [46] [47]. This includes the achieving

643 of more rapid regeneration rates in sorbent and larger $CO_2$ desorption capacities across
644 multiple adsorption-desorption cycles[25] [46] [47].

645 The dielectric response of the ACs will again be of key focus in guaranteeing suitable
646 regeneration, however temperatures applied for regeneration will likely take place at a
647 substantially lower temperature (~100 °C). Experimental tests with the MCC-based biochars
648 proved this temperature to be attainable without the use of MW-susceptor. Assuming that
649 activation will not negatively affect the AC dielectric properties, regeneration at such
650 temperature should be attainable. As highlighted previously, the use of a reduced sweeping
651 gas flow rate may be beneficial for desorption.

652 Complementing this development will also include comparing the adsorption-desorption
653 capability with other ACs outside of Norit R, for further confirmation of its effectiveness [11].
654 Nonetheless, in also factoring the benefit of MCC to the circular economy, this study has
655 established a promising AC development trajectory for a greener post-combustion capture
656 where emissions reduction is coupled with the sustainable utilisation of waste.

657 **4. Conclusions**

658 This study investigated, for the first time, the production of activated carbons from
659 microcrystalline cellulose, with the use of susceptor-assisted microwave heating during
660 activation. Comparing the MW-prepared ACs with those produced with conventional heating
661 in our previous work, at 200 °C higher temperature, presented an opportunity to assess the
662 production efficiency of MW heating. The MW-prepared ACs were shown to possess similar
663 characteristics to the conventionally-prepared ACs, particularly a shared substantial
664 microporosity, despite the more moderate activation temperature used. Amidst their similar

properties, the MW-prepared ACs possessed larger $CO_2$ adsorption capacities under both static and dynamic adsorption conditions, at equivalent activation burn-offs – 10, 20 and 30 wt %. Under dynamic conditions, MW-prepared ACs of 20 and 30 wt % burn-off possessed higher $CO_2$ adsorption capacities than commercial, $CO_2$-capturing AC Norit R, and displayed identical desorption capability (> 98 % full desorption).

Another key difference identified between these two types of AC was the enhanced basic surface character of MW-prepared-ACs, which occurred as a result of the MW heating profile along with the introduction of N-containing species into the ACs of 20 and 30 wt % burn-off during activation, due to reactions caused by hot spot formation and the $N_2$ atmosphere used in the reactor. Overall, using MW heating, ACs originating from a circular feedstock have been produced with reduced temperature, energy input and time, yet more favourable chemical and physical properties that promote greater $CO_2$ adsorption capacity.

**Acknowledgements**

For the purpose of open access, the author has applied a Creative Commons Attribution (CC-BY) licence to any Author Accepted Manuscript version arising from this submission.

Authors would like to thank The Leverhulme Trust for the funding provided through the Grant DS-2017-073. Simbarashe Biti, a Leverhulme Trust Doctoral Scholar, is part of the 15 PhD scholarships of the 'Leverhulme Centre for Doctoral Training in Sustainable Production of Chemicals and Materials' at the University of Aberdeen (Scotland, United Kingdom). Elemental analysis data was produced with the assistance of the analytical facilities in the School of Chemistry at the University of Birmingham.

**Authors contribution:**

687 S.B.: investigation, data curation and writing—original draft preparation; C.F.M and S.B.:
688 conceptualization, visualisation, and methodology; C.F.M., S.B., D.D., A. McC., and I.G.:
689 writing—review and editing; D.D. and C.F.M.: funding acquisition (D.D. lead of the funding
690 acquisition); C.F.M., D.D., A. McC., and I.G: supervision. All authors have read and agreed to
691 the published version of the manuscript.

692

# References


[1] A. Razzaq, A. Sharif, I. Ozturk, S. Afshan, Dynamic and threshold effects of energy transition and environmental governance on green growth in COP26 framework, Renewable and Sustainable Energy Reviews. 179 (2023) 113296. https://doi.org/10.1016/J.RSER.2023.113296.

[2] W.Y. Hong, A techno-economic review on carbon capture, utilisation and storage systems for achieving a net-zero CO2 emissions future, Carbon Capture Science & Technology. 3 (2022) 100044. https://doi.org/10.1016/J.CCST.2022.100044.

[3] S. Budinis, S. Krevor, N. Mac Dowell, N. Brandon, A. Hawkes, An assessment of CCS costs, barriers and potential, Energy Strategy Reviews. 22 (2018) 61–81. https://doi.org/10.1016/j.esr.2018.08.003.

[4] R.K. Singh, S.K. Mishra, B. Velramar, P.R. Kumar, Development of biologically-based activated carbon for advanced water and wastewater treatment process, Bioremediation of Pollutants: From Genetic Engineering to Genome Engineering. (2020) 215–225. https://doi.org/10.1016/B978-0-12-819025-8.00009-0.

[5] T. Fu, B. Zhang, X. Gao, S. Cui, C.-Y. Guan, Y. Zhang, B. Zhang, Y. Peng, Recent progresses, challenges, and opportunities of carbon-based materials applied in heavy metal polluted soil remediation, Science of the Total Environment. 856 (2023) 158810. https://doi.org/10.1016/j.scitotenv.2022.158810.

[6] A. Hamid, M. Fatah, W.B. Utomo, I.D. Febriana, Z. Rahmawati, Annafiyah, A.M. Ilmah, An Improvement of Catalytic Converter Activity Using Copper Coated Activated Carbon Derived from Banana Peel, International Journal of Renewable Energy Development. 12 (2023) 144–154. https://doi.org/10.14710/IJRED.2023.48739.

[7] K. Malini, D. Selvakumar, N.S. Kumar, Activated carbon from biomass: Preparation, factors improving basicity and surface properties for enhanced CO2 capture capacity – A review, Journal of CO2 Utilization. 67 (2023) 102318. https://doi.org/10.1016/J.JCOU.2022.102318.

[8] M.R. Ketabchi, S. Babamohammadi, W.G. Davies, M. Gorbounov, S. Masoudi Soltani, Latest advances and challenges in carbon capture using bio-based sorbents: A state-of-the-art review, Carbon Capture Science & Technology. 6 (2023) 100087. https://doi.org/10.1016/J.CCST.2022.100087.

[9] O.H.P. Gunawardene, C.A. Gunathilake, K. Vikrant, S.M. Amaraweera, Carbon Dioxide Capture through Physical and Chemical Adsorption Using Porous Carbon Materials: A Review, Atmosphere 2022, Vol. 13, Page 397. 13 (2022) 397. https://doi.org/10.3390/ATMOS13030397.

[10] A. Mukherjee, J.A. Okolie, A. Abdelrasoul, C. Niu, A.K. Dalai, Review of post-combustion carbon dioxide capture technologies using activated carbon, Journal of Environmental Sciences. 83 (2019) 46–63. https://doi.org/10.1016/J.JES.2019.03.014.

[11] S. Biti, A. Mccue, D. Dionisi, I. Graça, C.F. Martín, Sustainable microcrystalline cellulose-based activated carbons for a greener carbon capture at post-combustion conditions, International Journal of Greenhouse Gas Control. 125 (2023) 103876. https://doi.org/10.1016/J.IJGGC.2023.103876.

[12] G. Durán-Jiménez, J. Rodriguez, E.T. Kostas, L.A. Stevens, L. Lozada-Rodríguez, E. Binner, C. Dodds, Simultaneous conventional and microwave heating for the synthesis of adsorbents for CO2 capture: Comparative study to pristine technologies, Chemical Engineering Journal. 438 (2022). https://doi.org/10.1016/J.CEJ.2022.135549.

[13] Z. Peng, J.Y. Hwang, J. Mouris, R. Hutcheon, X. Sun, Microwave absorption characteristics of conventionally heated nonstoichiometric ferrous oxide, Metall Mater Trans A Phys Metall Mater Sci. 42 (2011) 2259–2263. https://doi.org/10.1007/S11661-011-0652-9/FIGURES/9.

[14] J. Xu, Microwave Pretreatment, Pretreatment of Biomass: Processes and Technologies. (2015) 157–172. https://doi.org/10.1016/B978-0-12-800080-9.00009-8.

[15] C. Gabriel, S. Gabriel, E.H. Grant, B.S.J. Halstead, D. Michael P Mingos, Dielectric parameters relevant to microwave dielectric heating, Chem Soc Rev. 27 (1998) 213–224. https://doi.org/10.1039/A827213Z.

[16] D. Trache, A. Donnot, K. Khimeche, R. Benelmir, N. Brosse, Physico-chemical properties and thermal stability of microcrystalline cellulose isolated from Alfa fibres, Carbohydr Polym. 104 (2014) 223–230. https://doi.org/10.1016/J.CARBPOL.2014.01.058.

[17] D. Trache, M.H. Hussin, C.T. Hui Chuin, S. Sabar, M.R.N. Fazita, O.F.A. Taiwo, T.M. Hassan, M.K.M. Haafiz, Microcrystalline cellulose: Isolation, characterization and bio-composites application—A review, Int J Biol Macromol. 93 (2016) 789–804. https://doi.org/10.1016/j.ijbiomac.2016.09.056.

[18] E. Galiwango, N.S. Abdel Rahman, A.H. Al-Marzouqi, M.M. Abu-Omar, A.A. Khaleel, Isolation and characterization of cellulose and α-cellulose from date palm biomass waste, Heliyon. 5 (2019) e02937. https://doi.org/10.1016/J.HELIYON.2019.E02937.

[19] C. Ellison, M. McKeown, S. Trabelsi, D. Boldor, Dielectric Properties of Biomass/Biochar Mixtures at Microwave Frequencies, Energies (Basel). 10 (2017) 502. https://doi.org/10.3390/en10040502.

[20] A.A. Abd, S.Z. Naji, A.S. Hashim, M.R. Othman, Carbon dioxide removal through physical adsorption using carbonaceous and non-carbonaceous adsorbents: A review, J Environ Chem Eng. 8 (2020) 104142. https://doi.org/10.1016/J.JECE.2020.104142.

[21] D.P. Vargas, L. Giraldo, J. Silvestre-Albero, J.C. Moreno-Piraján, CO2 adsorption on binderless activated carbon monoliths, Adsorption. 17 (2011) 497–504. https://doi.org/10.1007/s10450-010-9309-z.

[22] J.J. Manyà, B. González, M. Azuara, G. Arner, Ultra-microporous adsorbents prepared from vine shoots-derived biochar with high CO2 uptake and CO2/N2 selectivity, Chemical Engineering Journal. 345 (2018) 631–639. https://doi.org/10.1016/j.cej.2018.01.092.

[23] V. Bernal, L. Giraldo, J. Moreno-Piraján, Physicochemical Properties of Activated Carbon: Their Effect on the Adsorption of Pharmaceutical Compounds and Adsorbate–Adsorbent Interactions, C (Basel). 4 (2018) 62. https://doi.org/10.3390/c4040062.

[24] J.S. Noh, J.A. Schwarz, Estimation of the point of zero charge of simple oxides by mass titration, J Colloid Interface Sci. 130 (1989) 157–164. https://doi.org/10.1016/0021-9797(89)90086-6.

[25] M.M. Yassin, S. Biti, W. Afzal, C. Fernández Martín, A systematic analysis of the dynamics of microwave- and conventionally-assisted swing adsorption on zeolite 13X and an activated carbon under post-combustion carbon capture conditions, J Environ Chem Eng. 9 (2021) 106835. https://doi.org/10.1016/J.JECE.2021.106835.

[26] C. Erkey, M. Türk, Thermodynamics and kinetics of adsorption of metal complexes on surfaces from supercritical solutions, Supercritical Fluid Science and Technology. 8 (2021) 73–127. https://doi.org/10.1016/B978-0-444-64089-5.00047-0.

[27] C. Ma, J. Bai, M. Demir, X. Hu, S. Liu, L. Wang, Water chestnut shell-derived N/S-doped porous carbons and their applications in CO2 adsorption and supercapacitor, Fuel. 326 (2022) 125119. https://doi.org/10.1016/J.FUEL.2022.125119.

[28] M.Z. Abdullah, A. Qasim, Parametric Analysis of Carbon Dioxide Adsorption on Nanoporous Activated Carbon Using Computational Approach, Procedia Eng. C (2016) 1416–1422. https://doi.org/10.1016/J.PROENG.2016.06.626.

[29] F. Raganati, P. Ammendola, R. Chirone, CO2 capture performances of fine solid sorbents in a sound-assisted fluidized bed, Powder Technol. 268 (2014) 347–356. https://doi.org/10.1016/J.POWTEC.2014.08.062.

[30] C.F. Martín, M.G. Plaza, J.J. Pis, F. Rubiera, C. Pevida, T.A. Centeno, On the limits of CO2 capture capacity of carbons, Sep Purif Technol. 74 (2010) 225–229. https://doi.org/10.1016/J.SEPPUR.2010.06.009.

[31] D. Tsyganov, N. Bundaleska, J. Henriques, E. Felizardo, A. Dias, M. Abrashev, J. Kissovski, A.M.B. do Rego, A.M. Ferraria, E. Tatarova, Simultaneous Synthesis and Nitrogen Doping of Free-Standing Graphene Applying Microwave Plasma, Materials 2020, Vol. 13, Page 4213. 13 (2020) 4213. https://doi.org/10.3390/MA13184213.

[32] M.S. Shafeeyan, W.M.A.W. Daud, A. Houshmand, A. Arami-Niya, Ammonia modification of activated carbon to enhance carbon dioxide adsorption: Effect of pre-oxidation, Appl Surf Sci. 257 (2011) 3936–3942. https://doi.org/10.1016/j.apsusc.2010.11.127.

[33] W. Xing, C. Liu, Z. Zhou, L. Zhang, J. Zhou, S. Zhuo, Z. Yan, H. Gao, G. Wang, S. Zhang Qiao, ‡ W Xing, C. Liu, Superior CO 2 uptake of N-doped activated carbon through hydrogen-

bonding interaction †, This Journal Is [a] The Royal Society of Chemistry 2012 Energy Environ. Sci. 5 (2012) 7323. https://doi.org/10.1039/c2ee21653a.

[34] M.A.A. Zaini, M.J. Kamaruddin, Critical issues in microwave-assisted activated carbon preparation, J Anal Appl Pyrolysis. 101 (2013) 238–241. https://doi.org/10.1016/j.jaap.2013.02.003.

[35] F. Motasemi, A.A. Salema, M.T. Afzal, Dielectric characterization of corn stover for microwave processing technology, Fuel Processing Technology. (2015). https://doi.org/10.1016/j.fuproc.2014.12.006.

[36] F.X. Collard, J. Blin, A review on pyrolysis of biomass constituents: Mechanisms and composition of the products obtained from the conversion of cellulose, hemicelluloses and lignin, Renewable and Sustainable Energy Reviews. 38 (2014) 594–608. https://doi.org/10.1016/J.RSER.2014.06.013.

[37] M. Bartoli, M. Giorcelli, P. Jagdale, M. Rovere, A. Tagliaferro, M. Chae, D.C. Bressler, Shape tunability of carbonized cellulose nanocrystals, SN Appl Sci. 1 (2019). https://doi.org/10.1007/S42452-019-1727-2.

[38] Y.R. Rhim, D. Zhang, D.H. Fairbrother, K.A. Wepasnick, K.J. Livi, R.J. Bodnar, D.C. Nagle, Changes in electrical and microstructural properties of microcrystalline cellulose as function of carbonization temperature, Carbon N Y. 48 (2010) 1012–1024. https://doi.org/10.1016/J.CARBON.2009.11.020.

[39] S. Kumar N, D. Grekov, P. Pré, B.J. Alappat, Microwave mode of heating in the preparation of porous carbon materials for adsorption and energy storage applications – An overview, Renewable and Sustainable Energy Reviews. 124 (2020). https://doi.org/10.1016/J.RSER.2020.109743.

[40] C. Quan, R. Su, N. Gao, Preparation of activated biomass carbon from pine sawdust for supercapacitor and CO 2 capture, (2020). https://doi.org/10.1002/er.5206.

[41] N.A. Rashidi, S. Yusup, Potential of palm kernel shell as activated carbon precursors through single stage activation technique for carbon dioxide adsorption, J Clean Prod. 168 (2017) 474–486. https://doi.org/10.1016/J.JCLEPRO.2017.09.045.

[42] D.P. Bezerra, R.S. Oliveira, R.S. Vieira, C.L. Cavalcante, D.C.S. Azevedo, Adsorption of CO2 on nitrogen-enriched activated carbon and zeolite 13X, Adsorption 2011 17:1. 17 (2011) 235–246. https://doi.org/10.1007/S10450-011-9320-Z.

[43] J.A. Menéndez, A. Arenillas, B. Fidalgo, Y. Fernández, L. Zubizarreta, E.G. Calvo, J.M. Bermúdez, Microwave heating processes involving carbon materials, Fuel Processing Technology. 91 (2010) 1–8. https://doi.org/10.1016/j.fuproc.2009.08.021.

[44] C. Dhoke, A. Zaabout, S. Cloete, S. Amini, Review on Reactor Configurations for Adsorption-Based CO 2 Capture, (2021). https://doi.org/10.1021/acs.iecr.0c04547.

[45] F. Raganati, P. Ammendola, R. Chirone, On improving the CO2 recovery efficiency of a conventional TSA process in a sound assisted fluidized bed by separating heating and purging, Sep Purif Technol. 167 (2016) 24–31. https://doi.org/10.1016/J.SEPPUR.2016.05.001.

[46] F. Raganati, R. Chirone, P. Ammendola, CO2 Capture by Temperature Swing Adsorption: Working Capacity As Affected by Temperature and CO2 Partial Pressure, Ind Eng Chem Res. 59 (2020) 3593–3605. https://doi.org/10.1021/ACS.IECR.9B04901/ASSET/IMAGES/LARGE/IE9B04901_0006.JPEG.

[47] T. Chronopoulos, Y. Fernandez-Diez, M.M. Maroto-Valer, R. Ocone, D.A. Reay, Utilisation Of Microwave Energy for CO2 Desorption in Post-combustion Carbon Capture Using Solid Sorbents, Energy Procedia. 63 (2014) 2109–2115. https://doi.org/10.1016/J.EGYPRO.2014.11.227.